

Dependence of the fission half-lives of heavy nuclei on the highest proton magic number within a macro-microscopic approach

G. Royer ,* T. Boureau, and N. Potiron*Subatech Laboratory, UMR: IN2P3/CNRS-Université-IMT, 44 Nantes, France*

(Received 8 February 2023; accepted 14 August 2023; published 12 September 2023)

The potential barriers in the cold fission valley were determined within the original generalized liquid drop model, which takes into account the proximity energy, the charge and mass asymmetries, the microscopic shell and pairing corrections, and quasimolecular one- and two-body shapes. Due to microscopic effects and the proximity energy, double-humped fission barriers appear. The calculations were done within four hypotheses for the heaviest proton magic number: 114, 116, 118, and 120. The calculated partial or total fission half-lives of actinides and superheavy nuclei follow roughly the trend of the experimental data, the agreement being better for $Z = 118$.

DOI: [10.1103/PhysRevC.108.034307](https://doi.org/10.1103/PhysRevC.108.034307)

I. INTRODUCTION

The stability, sphericity, and mass of the ^{208}Pb nucleus allow one to consider that 82 and 126 are respectively the next proton and neutron magic numbers beyond 2, 8, 20, 28, 50 for protons and 82 for neutrons. The next neutron shell closure was predicted from the early shell model at $N = 184$ [1] and was confirmed by most of the recent calculations. For more than 50 years the next proton-shell closure has been positioned at $Z = 114$ [2,3]. More recently, the finite range droplet model [4] predicted a maximal negative shell correction for $Z = 114$ and $N = 178$. The mean field model [5] plunges the nucleons in a Woods-Saxon or Nilsson potential and leads to a small island of superheavy nuclei around $Z = 114$ and $N = 184$. The relativistic mean field approach uses an effective interaction which simulates the meson exchange [6] and predicts $Z = 120$ and $N = 172$ as the next proton and neutron magic numbers. The Hartree-Fock-Bogoliubov method approach uses Skyrme or Gogny forces and leads to $Z = 126$ and $N = 184$ [7]. The possible proton shell shift from 114 to $Z = 122$ has been advanced also [8]. The differences between the model predictions come mainly from the description of the spin-orbit coupling since the macroscopic liquid-drop barriers disappear for Z higher than around 103. Consequently, the shell effects dramatically influence the potential barrier of the heaviest nuclei and, with increasing proton and neutron numbers, the regions of nuclei stabilized by shell effects become poorly localized in particle number. A deformed minimum is also predicted around $Z = 108$ and $N = 152$ or 162.

Experimentally, most of the observed superheavy nuclei decay via α emission or simultaneous fission [9–11]. Theoretically, the spontaneous fission modes and lifetimes of superheavy elements have been deeply investigated within the nuclear density functional theory [12]. Using a generalized

liquid drop model with a modified proximity energy term [13,14], the decay modes of superheavy nuclei were predicted recently by comparing the half-lives of α emission and spontaneous fission and the experimental observations [13]. The same comparison has also been done [15] within a unified fission model and analytical formulas [16].

The purpose of this work is, for the actinide and superheavy nuclei, to compare the partial and total fission half-lives determined from the original version of the generalized liquid drop model [14] within four hypotheses for the heaviest proton magic number: 114, 116, 118, and 120. All possible mass and charge asymmetries are taken into account as well as the ellipsoidal deformations of the two different fission fragments, the proximity interaction, and the shell and pairing energies. The study is limited to quasimolecular shapes since these shapes are hardly accessible using the usual development of the nuclear radius.

II. GENERALIZED LIQUID DROP MODEL

The energy of a deformed nucleus is the sum of the GLDM energy and the microscopic energies. The GLDM energy is expressed as [14]

$$E = E_V + E_S + E_C + E_{\text{prox}}, \quad (1)$$

where the different terms are, respectively, the volume, surface, Coulomb, and proximity energies.

All along the fission path the proximity energy term E_{prox} takes into account the nuclear attractive forces between nucleons in regard in the neck or the gap between the nascent fragments. In the quasimolecular shape valley where the necks are narrow and well developed, this correction to the surface energy plays a main role on a large part of the fission path and especially around the touching point. The absence of this term leads to an unrealistic Coulomb peak. When the proximity energy is taken into account, the potential barrier is smooth.

*royer@subatech.in2p3.fr

The proximity energy is defined as

$$E_{\text{prox}}(r) = 2\gamma \int_{h_{\text{min}}}^{h_{\text{max}}} \Phi[D(r, h)/b] 2\pi h dh, \quad (2)$$

where r is the distance between the mass centers. Φ is the proximity function of Feldmeier [17]. h is the transverse distance in the neck relatively to the fission axis. h_{min} is zero for separated fragments or the neck radius for one-body shapes and h_{max} is the maximum value for which surfaces of the two nascent or separated fragments are still in regard. b the surface width fixed at 0.99 fm. D is the distance between the opposite surfaces on a line parallel to the fission axis. γ is the surface parameter.

The selected one-body shape sequence consists of two connected half-elliptic lemniscatoids, allowing the development of a deep neck while keeping almost spherical ends [14]. For a given final asymmetry, there is a one-to-one correspondence between the distance r between the centers of the future fragments and the shape of the deformed nucleus.

For one-body shapes, the first three contributions are given by

$$E_V = -15.494(1 - 1.8I^2)A \text{ MeV}, \quad (3)$$

$$E_S = 17.9439(1 - 2.6I^2)A^{2/3} \frac{S}{4\pi R_0^2} \text{ MeV}, \quad (4)$$

$$E_C = 0.6e^2(Z^2/R_0)B_C. \quad (5)$$

$I = (N - Z)/A$ is the relative neutron excess and S is the surface of the deformed nucleus. The Coulomb shape dependent function B_C was determined within the method proposed by Cohen and Swiatecki [18] using the axial symmetry of the system and complete elliptic integrals:

$$B_C = 0.5 \int [V(\theta)/V_0][R(\theta)/R_0]^3 \sin \theta d\theta. \quad (6)$$

$V(\theta)$ is the electrostatic potential at the surface and V_0 the surface potential of the sphere. The radius R_0 of the compound nucleus is given by $R_0 = (1.28A^{1/3} - 0.76 + 0.8A^{-1/3})$ fm. For two-body shapes, the coaxial ellipsoidal deformations were considered [19]. For a distance r between the mass centers of the fragments, the shape depends on two parameters: The ratios s_i ($i = 1, 2$) between the transverse semiaxis $a_i = R_i s_i^{1/3}$ and the radial semiaxis $c_i = R_i s_i^{-2/3}$ of the fragments. The prolate deformation is characterized by $s \leq 1$ and the eccentricity is $e^2 = 1 - s^2$, while in the oblate case $s \geq 1$ and $e^2 = 1 - s^{-2}$.

In the prolate case, the relative surface energy is given by

$$B_{S,i} = \frac{(1 - e_i^2)^{1/3}}{2} \left[1 + \frac{\sin^{-1}(e_i)}{e_i(1 - e_i^2)^{1/2}} \right] \quad (7)$$

and in the oblate case

$$B_{S,i} = \frac{(1 + \epsilon_i^2)^{1/3}}{2} \left[1 + \frac{\ln(\epsilon_i + (1 + \epsilon_i^2)^{1/2})}{\epsilon_i(1 + \epsilon_i^2)^{1/2}} \right], \quad (8)$$

$$\epsilon_i^2 = s_i^2 - 1.$$

The Coulomb self-energy of the spheroid i reads

$$E_{C,\text{self}} = \frac{3e^2 Z_i^2 B_{C,i}}{5R_i}. \quad (9)$$

The relative self-energy is, respectively, in the prolate and oblate cases

$$B_{C,i} = \frac{(1 - e_i^2)^{1/3}}{2e_i} \ln \frac{1 + e_i}{1 - e_i}, \quad (10)$$

$$B_{C,i} = \frac{(1 + \epsilon_i^2)^{1/3}}{\epsilon_i} \tan^{-1} \epsilon_i. \quad (11)$$

The Coulomb interaction energy between the two fragments is calculated as

$$E_{C,\text{int}} = \frac{e^2 Z_1 Z_2}{r} [s(\lambda_1) + s(\lambda_2) - 1 + S(\lambda_1, \lambda_2)],$$

$$\lambda_i^2 = \frac{c_i^2 - a_i^2}{r^2}. \quad (12)$$

In the prolate and oblate cases, $s(\lambda_i)$ is expressed as

$$s(\lambda_i) = \frac{3}{4} \left(\frac{1}{\lambda_i} - \frac{1}{\lambda_i^3} \right) \ln \left(\frac{1 + \lambda_i}{1 - \lambda_i} \right) + \frac{3}{2\lambda_i^2}, \quad (13)$$

$$s(\lambda_i) = \frac{3}{2} \left(\frac{1}{\omega_i} + \frac{1}{\omega_i^3} \right) \tan^{-1} \omega_i - \frac{3}{2\omega_i^2}, \quad \omega_i^2 = -\lambda_i^2. \quad (14)$$

$S(\lambda_1, \lambda_2)$ can be calculated within a twofold summation:

$$S(\lambda_1, \lambda_2) = \sum_{j=1}^{\infty} \sum_{k=1}^{\infty} \frac{3}{(2j+1)(2j+3)} \frac{3}{(2k+1)(2k+3)}$$

$$\times \frac{(2j+2k)!}{(2j)!(2k)!} \lambda_1^{2j} \lambda_2^{2k}. \quad (15)$$

This GLDM has been used to study the fission [20,21], fusion [14,22,23], and cluster [24,25] and α [16,26] reactions.

III. ANALYTICAL SHELL ENERGY

The shape-dependent shell corrections were calculated within the droplet model formulas [27] with slightly different values of the parameters. The shell energy is

$$E_{\text{shell}} = E_{\text{shell}}^{\text{sphere}} (1 - 3.1\theta^2) e^{-\theta^2}, \quad (16)$$

$$\theta^2 = (\delta R)^2 / a^2. \quad (17)$$

δR is the deviation of the nuclear surface from the sphere. The range a was chosen to be $0.286r_0$. The shell corrections for a spherical nucleus are given by

$$E_{\text{shell}}^{\text{sphere}} = 5.8[(F(N) + F(Z))/(0.5A)^{2/3} - 0.28A^{1/3}] \text{ MeV}, \quad (18)$$

where, for $M_{i-1} < X < M_i$, M_i being the magic numbers,

$$F(X) = q_i(X - M_{i-1}) - 0.6(X^{5/3} - M_{i-1}^{5/3}), \quad (19)$$

$$q_i = 0.6(M_i^{5/3} - M_{i-1}^{5/3}) / (M_i - M_{i-1}). \quad (20)$$

For the two-body shapes, the shell energy is the sum of the shell corrections of the fragments. This algebraic method to

calculate the shell effects is simple but gives, at least for ellipsoidal deformations, almost the same results as Strutinsky's method.

IV. PAIRING ENERGY

The pairing energy was determined with the following formulas given in [28].

For even Z , even N nuclei

$$E_{\text{Pairing}} = 0. \quad (21)$$

For even Z , odd N nuclei

$$E_{\text{Pairing}} = 4.8/N^{1/3}. \quad (22)$$

For odd Z , even N nuclei

$$E_{\text{Pairing}} = 4.8/Z^{1/3}. \quad (23)$$

For odd Z , odd N , and $N = Z$ nuclei

$$E_{\text{Pairing}} = 4.8/N^{1/3} + 4.8/Z^{1/3} - 6.6/A^{2/3} + 30/A. \quad (24)$$

For odd Z , odd N , and $N \neq Z$ nuclei

$$E_{\text{Pairing}} = 4.8/N^{1/3} + 4.8/Z^{1/3} - 6.6/A^{2/3}. \quad (25)$$

As a first approach, the pairing energy of the compound nucleus is constant till the scission and is the sum of the pairing energy of the two fragments after the separation. The rearrangement of the nuclear matter during the violent scission is poorly known. This simple approach adopted to determine the pairing energy has been sufficient to reproduce the peaks and wells of the multiple-humped barriers of actinides [21].

V. HALF-LIVES

Within this asymmetric fission model the decay constant is simply given by $\lambda = \nu_0 P$. The assault frequency ν_0 was taken as $\nu_0 = 10^{20} \text{ s}^{-1}$. The barrier penetrability P is calculated within the action integral

$$P = \exp \left[-\frac{2}{\hbar} \int_{r_{\text{in}}}^{r_{\text{out}}} \sqrt{2B(r)[E(r) - E_{\text{g.s.}}]} dr \right]. \quad (26)$$

The inertia $B(r)$ is related to the reduced mass by

$$B(r) = \mu \{1 + 24 \exp[-3.25(r - R_{\text{sph}})/R_0]\}, \quad (27)$$

where R_{sph} is the distance between the mass centers of the future fragments in the initial sphere, $R_{\text{sph}}/R_0 = 0.75$ in the symmetric case. Around the ground state the inertia is higher than the irrotational flow since large internal reorganization occurs at level crossings. The reduced mass is reached asymptotically. The formula (27) is a simplified version of the one proposed in Ref. [29]. The partial half-life for a specific decay channel i is related to the decay constant λ_i by $T_{1/2,i} = \frac{\ln 2}{\lambda_i}$. To determine the total fission decay constant $\lambda = \lambda_1 + \lambda_2 + \dots + \lambda_n$ the partial half-lives of all the possible spontaneous fission channels were calculated, and the total fission half-lives follow $T_{1/2} = \frac{\ln 2}{\lambda}$.

As an example, for ^{255}Db , the partial half-lives of the main fission channels are displayed in Fig. 1 as functions of the mass of the heaviest fragment and the charge of the two fragments. More precisely, from left to right in the figure,

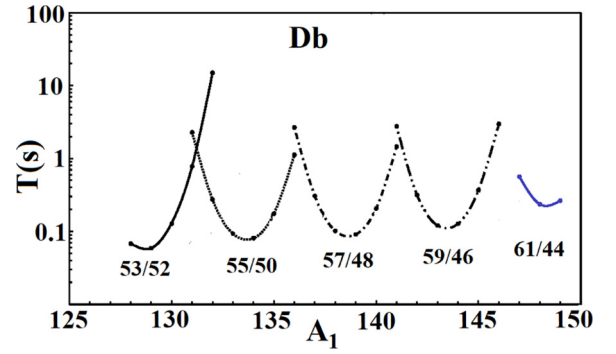


FIG. 1. Partial spontaneous fission half-lives (in s) of ^{255}Db as a function of the heaviest fragment mass number (A_1) and the different Z_1/Z_2 pairs of charges of the two fragments.

the solid black line, dotted line, and dashed-dotted line correspond respectively to the 53/52, 55/50, and 57/48 Z_1/Z_2 ratios. The dashed-double-dotted curve and heavy gray curve (three points) correspond to the 59/46 and 61/44 Z_1/Z_2 ratios. For a given pair (Z_1, Z_2) the half-lives are positioned on a nice parabola and vary as a function of the mass of the fragments.

VI. POTENTIAL BARRIERS

The potential barriers corresponding to the lowest partial half-life and consequently to the most probable fission path are displayed in Fig. 2 for several heavy and superheavy nuclei. The gray dashed-dotted line, the black solid line, the dotted line, the gray dashed line, the black solid line, the dashed black curve, and short dashed curve correspond to the ^{236}U , ^{243}Am , ^{248}Cm , ^{255}Es , ^{258}Rf , ^{259}Lr , and ^{286}Fl . The zero energy corresponds to the deformation energy of the initial spherical nucleus when the microscopic energies are not taken into account. The shell effects generate the deformed ground state. For ^{286}Fl the proximity of the next proton magic number leads to a quasispherical ground state. When the neck is formed, the proximity energy and the shell effects introduce progressively a plateau or a shallow second minimum. Later on, the second peak corresponds to the transition from

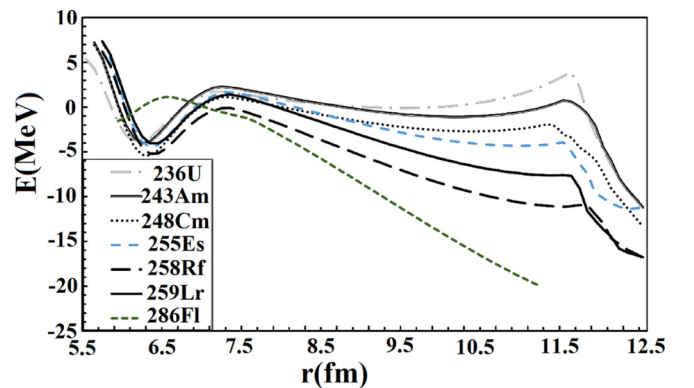


FIG. 2. Potential barriers for some actinide and superheavy nuclei as a function of the distance r between the mass centers of the fragments.

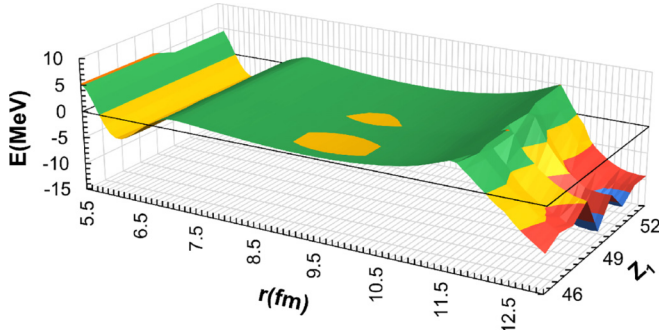


FIG. 3. Fission barriers for ^{236}U as a function of the asymmetry of the decay indicated by the charge of the heaviest fragment. The change of tint in the potential surface occurs every 5 MeV.

one-body quasimolecular shapes to two-body ellipsoidal shapes. In Fig. 3, for ^{236}U , the potential energy surface is displayed as functions of the charge number of the heaviest fragment and the distance between mass centers. In the figure, the change of gray tint occurs every 5 MeV. The height of the first maximum is quasiconstant since it depends mainly on the shell effects of the decaying nucleus. The height of the external maximum generally increases with the asymmetry but the shell effects in the fragments lead to favoring exit channels containing fragments close to the doubly magic $^{132}_{50}\text{Sn}$ nucleus. More precisely, in this example, Table I indicates the height of the second maximum as a function of the charge Z_1 of the heaviest fragment. The exit channel via the emission of a $^{130}_{50}\text{Sn}$ is favored. Figures 1, 2, and 3 are drawn considering $Z = 118$ as the next proton magic number.

VII. DEPENDENCE OF THE HALF-LIVES ON THE NEXT MAGIC PROTON NUMBER

In Tables II and III the experimental spontaneous fission half-lives of actinide and superheavy nuclei are compared with our predictions assuming 114, 116, 118, and 120 as the next proton magic number. The most probable exit channel is indicated in the first column for 114 and in the fifth column for $Z = 118$ and 120. It is not obvious whether the comparison must be done with the partial or the total theoretical fission half-lives, especially for the superheavy nuclei. So, the partial and total half-lives are compared in columns 6 and 7 for $Z = 118$. There is generally a factor of around 10 between the two values.

The root-mean-square deviations between the decimal logarithms of the theoretical and experimental half-lives of the actinides are respectively 3.89, 2.55, 2.68, and 4.22 for the partial half lives when $Z = 114, 116, 118,$ and 120 and 2.64 for the total half-lives when $Z = 118$.

TABLE I. Height of the second maximum (in MeV) of the fission barrier as a function of the charge of the heaviest fragment.

Z_1	46	47	48	49	50	51	52	53	54
Height	4.37	4.36	3.99	5.13	3.87	4.63	4.66	4.81	5.05

TABLE II. Comparison between experimental and theoretical spontaneous partial or total fission half-lives of actinide nuclei assuming 114, 116, 118, and 120 as the next proton magic number.

Reaction	$T_{\text{exp}}(\text{s})$	Partial T_{th}	
		$Z = 114$	$Z = 116$
$^{232}_{92}\text{U} \rightarrow ^{134}_{52}\text{Te} + ^{98}_{40}\text{Zr}$	2.5×10^{21}	4.8×10^{18}	1.3×10^{20}
$^{234}_{92}\text{U} \rightarrow ^{134}_{52}\text{Te} + ^{100}_{40}\text{Zr}$	4.7×10^{23}	4.6×10^{19}	1.1×10^{21}
$^{235}_{92}\text{U} \rightarrow ^{131}_{50}\text{Sn} + ^{104}_{42}\text{Mo}$	3.1×10^{26}	1.1×10^{24}	2.0×10^{25}
$^{236}_{92}\text{U} \rightarrow ^{130}_{50}\text{Sn} + ^{106}_{42}\text{Mo}$	7.8×10^{23}	1.7×10^{22}	5.4×10^{23}
$^{238}_{92}\text{U} \rightarrow ^{130}_{50}\text{Sn} + ^{108}_{42}\text{Mo}$	2.6×10^{23}	5.2×10^{23}	1.1×10^{25}
$^{239}_{94}\text{Pu} \rightarrow ^{130}_{50}\text{Sn} + ^{109}_{44}\text{Ru}$	2.5×10^{23}	9.9×10^{22}	4.1×10^{24}
$^{240}_{94}\text{Pu} \rightarrow ^{128}_{50}\text{Sn} + ^{112}_{44}\text{Ru}$	3.7×10^{18}	2.3×10^{20}	1.2×10^{22}
$^{241}_{94}\text{Pu} \rightarrow ^{128}_{50}\text{Sn} + ^{113}_{44}\text{Ru}$	2.3×10^{24}	2.6×10^{21}	1.3×10^{23}
$^{243}_{95}\text{Am} \rightarrow ^{133}_{51}\text{Sb} + ^{110}_{44}\text{Ru}$	6.3×10^{21}	3.6×10^{22}	2.0×10^{24}
$^{243}_{96}\text{Cm} \rightarrow ^{122}_{48}\text{Cd} + ^{121}_{48}\text{Cd}$	1.7×10^{19}	2.3×10^{16}	6.0×10^{18}
$^{245}_{96}\text{Cm} \rightarrow ^{130}_{50}\text{Sn} + ^{115}_{46}\text{Pd}$	4.4×10^{19}	2.0×10^{20}	2.2×10^{22}
$^{248}_{96}\text{Cm} \rightarrow ^{130}_{50}\text{Sn} + ^{118}_{46}\text{Pd}$	1.3×10^{14}	1.9×10^{18}	2.3×10^{20}
$^{249}_{97}\text{Bk} \rightarrow ^{128}_{50}\text{Sn} + ^{121}_{47}\text{Ag}$	6.1×10^{16}	6.5×10^{15}	1.9×10^{18}
$^{249}_{98}\text{Cf} \rightarrow ^{127}_{50}\text{Sn} + ^{122}_{48}\text{Cd}$	2.2×10^{18}	4.8×10^{10}	1.9×10^{14}
$^{250}_{98}\text{Cf} \rightarrow ^{125}_{49}\text{In} + ^{125}_{49}\text{In}$	5.2×10^{11}	4.2×10^{11}	1.2×10^{15}
$^{253}_{99}\text{Es} \rightarrow ^{128}_{50}\text{Sn} + ^{125}_{49}\text{In}$	2.0×10^{13}	6.5×10^6	3.7×10^9
$^{255}_{99}\text{Es} \rightarrow ^{128}_{50}\text{Sn} + ^{127}_{49}\text{In}$	8.4×10^{10}	5.5×10^6	3.5×10^9
$^{250}_{100}\text{Fm} \rightarrow ^{125}_{50}\text{Sn} + ^{125}_{50}\text{Sn}$	2.6×10^7	1.8×10^3	4.3×10^5
$^{252}_{100}\text{Fm} \rightarrow ^{126}_{50}\text{Sn} + ^{126}_{50}\text{Sn}$	4.0×10^9	1.0×10^4	2.8×10^6
$^{254}_{100}\text{Fm} \rightarrow ^{127}_{50}\text{Sn} + ^{127}_{50}\text{Sn}$	1.9×10^7	1.9×10^4	5.6×10^6
$^{256}_{100}\text{Fm} \rightarrow ^{128}_{50}\text{Sn} + ^{128}_{50}\text{Sn}$	1.0×10^4	1.1×10^4	3.2×10^6
$^{255}_{101}\text{Md} \rightarrow ^{129}_{51}\text{Sb} + ^{126}_{50}\text{Sn}$	1.1×10^6	1.8×10^2	4.1×10^4
$^{257}_{101}\text{Md} \rightarrow ^{130}_{51}\text{Sb} + ^{127}_{50}\text{Sn}$	2.0×10^6	1.1×10^3	2.7×10^4
$^{259}_{101}\text{Md} \rightarrow ^{130}_{51}\text{Sb} + ^{129}_{50}\text{Sn}$	5.8×10^3	7.7×10^{-1}	1.3×10^3
$^{252}_{102}\text{No} \rightarrow ^{126}_{51}\text{Sb} + ^{126}_{51}\text{Sb}$	1.2×10^1	2.5×10^{-1}	4.3×10^1
$^{254}_{102}\text{No} \rightarrow ^{127}_{51}\text{Sb} + ^{127}_{51}\text{Sb}$	3.0×10^4	1.1×10^0	1.9×10^2
$^{256}_{102}\text{No} \rightarrow ^{128}_{51}\text{Sb} + ^{128}_{51}\text{Sb}$	1.1×10^2	1.9×10^0	3.7×10^2
$^{257}_{102}\text{No} \rightarrow ^{129}_{51}\text{Sb} + ^{128}_{51}\text{Sb}$	1.7×10^3	2.1×10^0	4.3×10^2
$^{259}_{102}\text{No} \rightarrow ^{130}_{52}\text{Te} + ^{129}_{50}\text{Sn}$	3.5×10^4	3.7×10^0	1.1×10^2
$^{252}_{103}\text{Lr} \rightarrow ^{127}_{51}\text{Te} + ^{125}_{51}\text{Sb}$	3.6×10^1	1.6×10^{-3}	2.6×10^{-1}
$^{253}_{103}\text{Lr} \rightarrow ^{128}_{52}\text{Te} + ^{125}_{51}\text{Sb}$	2.9×10^1	5.0×10^{-3}	8.2×10^{-1}
$^{255}_{103}\text{Lr} \rightarrow ^{130}_{52}\text{Te} + ^{125}_{51}\text{Sb}$	2.2×10^4	2.0×10^{-2}	8.9×10^0
$^{256}_{103}\text{Lr} \rightarrow ^{132}_{53}\text{I} + ^{124}_{50}\text{Sn}$	9.0×10^5	3.6×10^{-2}	6.7×10^0
$^{257}_{103}\text{Lr} \rightarrow ^{132}_{53}\text{I} + ^{125}_{50}\text{Sn}$	2.2×10^3	4.3×10^{-2}	8.2×10^0
$^{259}_{103}\text{Lr} \rightarrow ^{132}_{53}\text{I} + ^{127}_{50}\text{Sn}$	5.8×10^3	1.3×10^{-3}	1.3×10^0
Reaction	Partial T_{th}	Total T_{th}	Partial T_{th}
	$Z = 118$	$Z = 118$	$Z = 120$
$^{232}_{92}\text{U} \rightarrow ^{120}_{48}\text{Cd} + ^{112}_{44}\text{Ru}$	1.1×10^{19}	3.5×10^{17}	3.6×10^{20}
$^{234}_{92}\text{U} \rightarrow ^{128}_{50}\text{Sn} + ^{106}_{42}\text{Mo}$	3.3×10^{21}	1.2×10^{21}	7.2×10^{22}
$^{235}_{92}\text{U} \rightarrow ^{128}_{50}\text{Sn} + ^{107}_{42}\text{Mo}$	1.8×10^{23}	3.5×10^{22}	7.5×10^{25}
$^{236}_{92}\text{U} \rightarrow ^{128}_{50}\text{Sn} + ^{108}_{42}\text{Mo}$	5.5×10^{23}	3.25×10^{23}	1.1×10^{25}
$^{238}_{92}\text{U} \rightarrow ^{130}_{50}\text{Sn} + ^{108}_{42}\text{Mo}$	2.0×10^{26}	9.4×10^{25}	3.3×10^{27}
$^{239}_{94}\text{Pu} \rightarrow ^{127}_{50}\text{Sn} + ^{112}_{44}\text{Ru}$	7.5×10^{22}	1.8×10^{22}	3.4×10^{24}
$^{240}_{94}\text{Pu} \rightarrow ^{134}_{52}\text{Te} + ^{106}_{42}\text{Mo}$	1.3×10^{23}	9.1×10^{22}	2.2×10^{25}
$^{241}_{94}\text{Pu} \rightarrow ^{134}_{52}\text{Te} + ^{107}_{42}\text{Mo}$	4.3×10^{24}	1.1×10^{24}	2.1×10^{26}
$^{243}_{95}\text{Am} \rightarrow ^{128}_{50}\text{Sn} + ^{115}_{45}\text{Rh}$	4.8×10^{23}	1.3×10^{23}	2.6×10^{25}

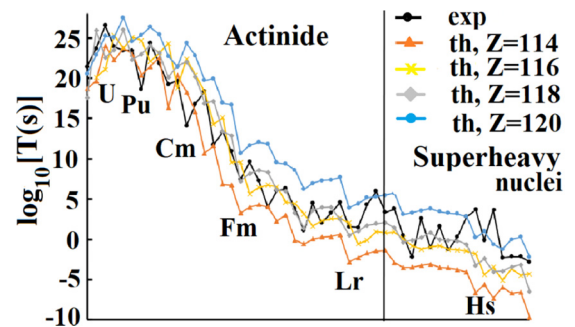
TABLE II. (Continued.)

Reaction	$T_{\text{exp}}(s)$	Partial T_{th}	Partial T_{th}
		$Z = 114$	$Z = 116$
$^{243}_{96}\text{Cm} \rightarrow ^{127}_{50}\text{Sn} + ^{116}_{46}\text{Pd}$	4.6×10^{20}	1.3×10^{20}	5.0×10^{22}
$^{245}_{96}\text{Cm} \rightarrow ^{128}_{50}\text{Sn} + ^{117}_{46}\text{Pd}$	9.5×10^{21}	3.3×10^{21}	9.0×10^{23}
$^{248}_{96}\text{Cm} \rightarrow ^{130}_{50}\text{Sn} + ^{118}_{46}\text{Pd}$	2.5×10^{22}	1.1×10^{22}	2.1×10^{24}
$^{249}_{97}\text{Bk} \rightarrow ^{128}_{50}\text{Sn} + ^{121}_{47}\text{Ag}$	4.0×10^{20}	1.5×10^{20}	5.9×10^{22}
$^{249}_{98}\text{Cf} \rightarrow ^{127}_{50}\text{Te} + ^{122}_{48}\text{Cd}$	1.4×10^{17}	7.2×10^{16}	5.0×10^{19}
$^{250}_{98}\text{Cf} \rightarrow ^{128}_{50}\text{Sn} + ^{122}_{48}\text{Cd}$	2.4×10^{17}	1.4×10^{17}	8.3×10^{19}
$^{253}_{99}\text{Es} \rightarrow ^{128}_{50}\text{Sn} + ^{125}_{49}\text{In}$	4.2×10^{13}	2.2×10^{13}	8.2×10^{16}
$^{255}_{99}\text{Es} \rightarrow ^{129}_{50}\text{Sn} + ^{126}_{49}\text{In}$	2.2×10^{13}	7.55×10^{12}	5.1×10^{16}
$^{250}_{100}\text{Fm} \rightarrow ^{125}_{50}\text{Sn} + ^{125}_{50}\text{Sn}$	1.2×10^8	1.7×10^7	4.5×10^{10}
$^{252}_{100}\text{Fm} \rightarrow ^{126}_{50}\text{Sn} + ^{126}_{50}\text{Sn}$	9.5×10^8	1.5×10^8	4.4×10^{11}
$^{254}_{100}\text{Fm} \rightarrow ^{127}_{50}\text{Sn} + ^{127}_{50}\text{Sn}$	2.0×10^9	3.7×10^8	1.1×10^{12}
$^{256}_{100}\text{Fm} \rightarrow ^{128}_{50}\text{Sn} + ^{128}_{50}\text{Sn}$	1.2×10^9	2.3×10^8	6.4×10^{11}
$^{255}_{101}\text{Md} \rightarrow ^{129}_{51}\text{Sb} + ^{126}_{50}\text{Sn}$	1.1×10^7	1.3×10^6	3.3×10^9
$^{257}_{101}\text{Md} \rightarrow ^{130}_{51}\text{Sb} + ^{127}_{50}\text{Sn}$	7.4×10^6	9.3×10^5	2.3×10^9
$^{259}_{101}\text{Md} \rightarrow ^{133}_{52}\text{Te} + ^{126}_{49}\text{In}$	3.0×10^3	2.0×10^3	3.9×10^8
$^{252}_{102}\text{No} \rightarrow ^{126}_{51}\text{Sb} + ^{126}_{51}\text{Sb}$	7.8×10^3	2.5×10^1	1.6×10^6
$^{254}_{102}\text{No} \rightarrow ^{127}_{51}\text{Sb} + ^{127}_{51}\text{Sb}$	4.1×10^4	4.2×10^3	9.2×10^6
$^{256}_{102}\text{No} \rightarrow ^{128}_{51}\text{Sb} + ^{128}_{51}\text{Sb}$	8.0×10^4	8.8×10^3	1.9×10^7
$^{257}_{102}\text{No} \rightarrow ^{129}_{51}\text{Sb} + ^{128}_{51}\text{Sb}$	9.7×10^4	9.75×10^3	2.4×10^7
$^{259}_{102}\text{No} \rightarrow ^{133}_{53}\text{I} + ^{126}_{49}\text{In}$	4.6×10^2	2.9×10^2	5.1×10^7
$^{252}_{103}\text{Lr} \rightarrow ^{127}_{52}\text{Te} + ^{125}_{51}\text{Sb}$	4.5×10^1	3.3×10^0	8.1×10^3
$^{253}_{103}\text{Lr} \rightarrow ^{128}_{52}\text{Te} + ^{125}_{51}\text{Sb}$	1.4×10^2	1.05×10^1	2.7×10^4
$^{255}_{103}\text{Lr} \rightarrow ^{129}_{52}\text{Te} + ^{126}_{51}\text{Sb}$	6.6×10^2	5.3×10^1	1.4×10^5
$^{256}_{103}\text{Lr} \rightarrow ^{129}_{52}\text{Te} + ^{127}_{51}\text{Sb}$	9.5×10^2	8.6×10^1	2.0×10^5
$^{257}_{103}\text{Lr} \rightarrow ^{130}_{52}\text{Te} + ^{127}_{51}\text{Sb}$	1.3×10^3	1.2×10^2	2.8×10^5
$^{259}_{103}\text{Lr} \rightarrow ^{131}_{53}\text{I} + ^{128}_{50}\text{Sn}$	2.3×10^2	2.5×10^1	5.3×10^5

The root-mean-square deviations between the decimal logarithms of the theoretical and experimental half-lives of these superheavy nuclei are respectively 4.66, 2.67, 1.73, and 2.85 for the partial half lives when $Z = 114, 116, 118,$ and 120 and 2.06 for the total half-lives when $Z = 118$. For all the actinide and superheavy nuclei the rms deviations are respectively 4.11, 2.58, 2.46, and 3.90 for the partial half lives when $Z = 114, 116, 118,$ and 120 and 2.5 for the total half-lives when $Z = 118$. These deviations are displayed in Fig. 4. For one isotope, the experimental and the four theoretical data are given on a vertical line. Some isotopes are indicated on the figure. The isotopes are arranged from the lightest actinide nuclei on the left to the heaviest superheavy nuclei on the right. The hypothesis of a next proton magic number of $Z = 114$ (indicated by gray solid triangles on the figure) leads generally to lower half-lives than the experimental values (black dots) of the actinide and superheavy nuclei while, with $Z = 120$ (grey dots), the predicted values for the actinides are generally too high. The hypotheses $Z = 116$ (crosses) or $Z = 118$ (diamond shaped symbols) lead to comparable deviations for the actinides but $Z = 118$ lowers the deviations for the superheavy nuclei. Nevertheless, in various regions different values of Z are better at reproducing experimental data. This confirms that

TABLE III. Comparison between experimental and theoretical spontaneous partial or total fission half-lives of superheavy nuclei assuming 114, 116, 118, or 120 as proton magic number.

Reaction	$T_{\text{exp}}(s)$	Partial T_{th}	Partial T_{th}
		$Z = 114$	$Z = 116$
$^{255}_{104}\text{Rf} \rightarrow ^{134}_{54}\text{Xe} + ^{121}_{50}\text{Sn}$	3.2×10^0	3.1×10^{-4}	1.5×10^{-1}
$^{256}_{104}\text{Rf} \rightarrow ^{128}_{52}\text{Te} + ^{128}_{52}\text{Te}$	6.4×10^{-3}	3.5×10^{-4}	5.6×10^{-2}
$^{257}_{104}\text{Rf} \rightarrow ^{128}_{52}\text{Te} + ^{129}_{52}\text{Te}$	3.9×10^2	6.0×10^{-4}	1.1×10^{-1}
$^{258}_{104}\text{Rf} \rightarrow ^{129}_{52}\text{Te} + ^{129}_{52}\text{Te}$	9.4×10^{-2}	8.2×10^{-4}	1.6×10^{-1}
$^{259}_{104}\text{Rf} \rightarrow ^{130}_{52}\text{Te} + ^{129}_{52}\text{Te}$	4.0×10^1	3.3×10^{-4}	5.9×10^{-2}
$^{260}_{104}\text{Rf} \rightarrow ^{130}_{52}\text{Te} + ^{130}_{52}\text{Te}$	5.1×10^{-2}	2.8×10^{-4}	4.7×10^{-2}
$^{262}_{104}\text{Rf} \rightarrow ^{131}_{52}\text{Te} + ^{131}_{52}\text{Te}$	2.1×10^0	1.8×10^{-4}	3.5×10^{-2}
$^{263}_{104}\text{Rf} \rightarrow ^{132}_{52}\text{Te} + ^{131}_{52}\text{Te}$	6.6×10^2	8.3×10^{-5}	1.6×10^{-2}
$^{255}_{105}\text{Db} \rightarrow ^{129}_{53}\text{I} + ^{126}_{52}\text{Te}$	8.0×10^{-1}	2.5×10^{-6}	3.6×10^{-4}
$^{258}_{106}\text{Sg} \rightarrow ^{130}_{53}\text{Xe} + ^{128}_{52}\text{Te}$	5.2×10^{-3}	1.1×10^{-6}	2.2×10^{-4}
$^{260}_{106}\text{Sg} \rightarrow ^{130}_{53}\text{I} + ^{130}_{53}\text{I}$	7.2×10^{-3}	2.1×10^{-7}	3.4×10^{-5}
$^{262}_{106}\text{Sg} \rightarrow ^{131}_{53}\text{I} + ^{131}_{53}\text{I}$	7.2×10^{-3}	2.9×10^{-7}	5.2×10^{-5}
$^{266}_{106}\text{Sg} \rightarrow ^{133}_{53}\text{I} + ^{133}_{53}\text{I}$	2.0×10^{-1}	1.6×10^{-8}	4.0×10^{-6}
$^{264}_{108}\text{Hs} \rightarrow ^{132}_{54}\text{Xe} + ^{132}_{54}\text{Xe}$	4.5×10^{-4}	2.1×10^{-10}	3.5×10^{-8}
Reaction		Partial T_{th}	Total T_{th}
		$Z = 118$	$Z = 118$
$^{255}_{104}\text{Rf} \rightarrow ^{128}_{52}\text{Te} + ^{127}_{52}\text{Te}$	6.2×10^0	4.1×10^{-1}	1.2×10^3
$^{256}_{104}\text{Rf} \rightarrow ^{128}_{52}\text{Te} + ^{128}_{52}\text{Te}$	9.7×10^0	8.2×10^{-1}	1.9×10^3
$^{257}_{104}\text{Rf} \rightarrow ^{128}_{52}\text{Te} + ^{129}_{52}\text{Te}$	1.9×10^1	1.5×10^0	3.7×10^3
$^{258}_{104}\text{Rf} \rightarrow ^{129}_{52}\text{Te} + ^{129}_{52}\text{Te}$	3.1×10^1	7.1×10^0	6.3×10^3
$^{259}_{104}\text{Rf} \rightarrow ^{130}_{52}\text{Te} + ^{129}_{52}\text{Te}$	1.4×10^1	8.5×10^{-1}	2.6×10^3
$^{260}_{104}\text{Rf} \rightarrow ^{130}_{52}\text{Te} + ^{130}_{52}\text{Te}$	8.7×10^0	7.7×10^{-1}	1.7×10^3
$^{262}_{104}\text{Rf} \rightarrow ^{131}_{52}\text{Te} + ^{131}_{52}\text{Te}$	7.1×10^0	6.1×10^{-1}	1.5×10^3
$^{263}_{104}\text{Rf} \rightarrow ^{132}_{52}\text{Te} + ^{131}_{52}\text{Te}$	3.1×10^0	2.4×10^{-1}	6.7×10^2
$^{255}_{105}\text{Db} \rightarrow ^{129}_{53}\text{I} + ^{126}_{52}\text{Te}$	5.9×10^{-2}	4.0×10^{-3}	9.4×10^0
$^{258}_{106}\text{Sg} \rightarrow ^{136}_{56}\text{Ba} + ^{122}_{50}\text{Sn}$	4.1×10^{-4}	1.2×10^{-4}	5.5×10^{-2}
$^{260}_{106}\text{Sg} \rightarrow ^{130}_{53}\text{I} + ^{130}_{53}\text{I}$	5.3×10^{-3}	4.0×10^{-4}	9.5×10^{-1}
$^{262}_{106}\text{Sg} \rightarrow ^{131}_{53}\text{I} + ^{131}_{53}\text{I}$	9.5×10^{-3}	7.0×10^{-4}	1.9×10^0
$^{266}_{106}\text{Sg} \rightarrow ^{133}_{53}\text{I} + ^{133}_{53}\text{I}$	5.2×10^{-4}	3.8×10^{-5}	1.1×10^{-1}
$^{264}_{108}\text{Hs} \rightarrow ^{135}_{56}\text{Ba} + ^{129}_{52}\text{Te}$	3.0×10^{-6}	3.4×10^{-7}	6.6×10^{-3}

FIG. 4. Comparison between experimental and theoretical decimal logarithm $\log_{10}[T(s)]$ of the fission half-lives assuming a proton magic number of 114, 116, 118, or 120.

the gap between the shells is narrow for the heaviest nuclei. Furthermore the experimental data have large error bars for the superheavy nuclei.

VIII. SUMMARY AND CONCLUSION

The deformation energy of fissioning nuclei was determined using the original generalized liquid drop model, which takes into account the proximity energy, the charge and mass

asymmetries, the microscopic corrections, and quasimolecular one- and two-body shapes. Due to shell effects and proximity energy, double-humped fission barriers appear. The calculations were done within four hypotheses for the heaviest proton magic number: 114, 116, 118, and 120. The calculated partial or total spontaneous fission half-lives of actinide and superheavy nuclei follow roughly the trend of the experimental data. The agreement is better for $Z = 118$ within our simple approach.

-
- [1] M. Göppert-Mayer and H. D. Jensen, *Elementary Theory of Nuclear Shell Structure* (Wiley, New York, 1955).
- [2] A. Sobczewski, F. Gareev, and B. N. Kalinkin, *Phys. Lett.* **22**, 500 (1966).
- [3] H. Meldner, *Ark. Fys.* **36**, 593 (1967).
- [4] P. Möller, J. R. Nix, W. D. Myers, and W. J. Swiatecki, *At. Data Nucl. Data Tables* **59**, 185 (1995).
- [5] S. Cwiok, J. Dobaczewski, P. H. Heenen, P. Magierski, and W. Nazarewicz, *Nucl. Phys. A* **611**, 211 (1996).
- [6] M. Bender, W. Nazarewicz, and P. G. Reinhard, *Phys. Lett. B* **515**, 42 (2001).
- [7] J. F. Berger, L. Bitaud, J. Dechargé, M. Girod, and K. Dietrich, *Nucl. Phys. A* **685**, 1 (2001).
- [8] P. Armbruster, *Eur. Phys. J. A* **37**, 159 (2008).
- [9] D. N. Poenaru and W. Greiner, *Experimental Techniques in Nuclear Physics* (Walter de Gruyter, Berlin, 1997).
- [10] J. H. Hamilton, S. Hofmann, and Yu. Ts. Oganessian, *Annu. Rev. Nucl. Part. Sci.* **63**, 383 (2013).
- [11] W. Thoennessen, *At. Data Nucl. Data Tables* **99**, 312 (2013).
- [12] A. Staszczak, A. Baran, and W. Nazarewicz, *Phys. Rev. C* **87**, 024320 (2013).
- [13] K. P. Santhosh, C. Nithya, and T. A. Jose, *Phys. Rev. C* **104**, 024617 (2021).
- [14] G. Royer and B. Remaud, *Nucl. Phys. A* **444**, 477 (1985).
- [15] X. J. Bao, S. Q. Guo, H. F. Zhang, Y. Z. Xing, J. M. Dong, and J. Q. Li, *J. Phys. G: Nucl. Part. Phys.* **42**, 085101 (2015).
- [16] G. Royer, *J. Phys. G: Nucl. Part. Phys.* **26**, 1149 (2000).
- [17] H. Feldmeier, in *Proceedings of the 12th Summer School on Nuclear Physics*, Mikolajki, Poland, 1979 (unpublished).
- [18] S. Cohen and W. J. Swiatecki, *Ann. Phys. (NY)* **22**, 406 (1963).
- [19] G. Royer and C. Piller, *J. Phys. G: Nucl. Part. Phys.* **18**, 1805 (1992).
- [20] G. Royer and B. Remaud, *J. Phys. G* **10**, 1541 (1984).
- [21] G. Royer, M. Jaffré, and D. Moreau, *Phys. Rev. C* **86**, 044326 (2012).
- [22] G. Royer, M. Guillot, and J. Monard, *Nucl. Phys. A* **1010**, 122191 (2021).
- [23] G. Royer, *Heavy Elements and Related New Phenomena* (World Scientific, Singapore, 1999), Vol. 1, pp 591–631.
- [24] G. Royer, R. K. Gupta, and V. Yu. Denisov, *Nucl. Phys. A* **632**, 275 (1998).
- [25] G. Royer, *Phys. Rev. C* **106**, 034605 (2022).
- [26] J. G. Deng, H. F. Zhang, and G. Royer, *Phys. Rev. C* **101**, 034307 (2020).
- [27] W. D. Myers, *Droplet Model of Atomic Nuclei* (Plenum, New York, 1977).
- [28] W. D. Myers and W. J. Swiatecki, *Nucl. Phys. A* **601**, 141 (1996).
- [29] P. Möller, J. R. Nix, and W. J. Swiatecki, *Nucl. Phys. A* **492**, 349 (1989).